Scanning Electrochemical Microscopy. 25. Application to Investigation of the Kinetics of Heterogeneous Electron Transfer at Semiconductor (WSe₂ and Si) Electrodes

Benjamin R. Horrocks,† Michael V. Mirkin,‡ and Allen J. Bard*

Department of Chemistry and Biochemistry, The University of Texas at Austin, Austin, Texas 78712

Received: December 28, 1993; In Final Form: April 6, 1994⊗

The measurement of the kinetics of electron transfer in the dark to various outer-sphere redox couples at both n- and p-WSe₂ electrodes in aqueous electrolytes and at n-Si in acetonitrile and methanol by scanning electrochemical microscopy (SECM) is reported. The absence of errors due to ohmic resistance, charging currents, and relative insensitivity of the method to parallel processes, such as corrosion, is shown to give the SECM approach advantages over more traditional electrochemical methods of measurement. Only one case, oxidation of $Ru(NH_3)_6^{2+}$ on p-WSe₂, exhibited an apparent transfer coefficient of 1, in agreement with theories that assume an ideal semiconductor/solution interface. The standard heterogeneous rate constant in 0.5 M Na_2SO_4 was $(1.7 \pm 0.6) \times 10^{-16}$ cm s⁻¹, independent of concentration in the range 1–5 mM, in rough agreement with theoretical estimates. In general, other redox couples showed low values (0.1–0.4) of the transfer coefficient, including the reduction of $Ru(NH_3)_6^{3+}$ on n-WSe₂, contrary to theoretical expectations of 1 for a semiconductor in depletion or 0.5 for a degenerate semiconductor. The SECM was also used to observe the different kinetics of $Ru(NH_3)_6^{2+}$ oxidation at step edges compared to the van der Waals surface. At steps, significant oxidation currents were observed even with the p-WSe₂ biased 0.4 V negative of the flatband potential. The low apparent transfer coefficients commonly found for dark processes at semiconductors are explained as the result of averaging over sites of different reactivity (steps, cracks, pits, and the van der Waals surface). The reduction of ferrocenium and N,N,N',N'-tetramethyl-1,4-phenylene diamine cation radical (TMPD·⁺) on n-Si in acetonitrile also exhibited transfer coefficients of about 0.3, whereas the transfer coefficient for the reduction of TMPD·⁺ in methanol was 0.6. In methanol, ferrocenium reacted with Si and so was reduced by a purely chemical mechanism, with a heterogeneous rate constant greater than 0.37 cm s⁻¹ and concurrent etching of the semiconductor.

Introduction

Although a vast literature concerning semiconductor electrodes and photoelectrochemistry exists,[1-6] relatively few measurements of heterogeneous electron-transfer rates to dissolved redox couples at nonilluminated electrodes have been reported.[7-20] The current–potential ($i–E$) curve at a dark semiconductor electrode (e.g., for the oxidation of a reduced species, Red, at a p-type semiconductor) is given by an expression governed by the bimolecular reaction between the majority carriers at the surface of the semiconductor and the redox couple:

$$i = nFAk_{et}p_{so}[\text{Red}] \qquad (1)$$

where p_{so} (cm⁻³) is the concentration of majority carriers at the surface (holes in this case), [Red] (mol cm⁻³) is the concentration of the reduced form of the redox couple, and k_{et} (cm⁴ s⁻¹) is a bimolecular electron-transfer rate constant. For example, the dependence of i on E, expressed as the apparent transfer coefficient, α, is a function of the variations of p_{so} and k_{et} with E. For redox couples with $E°$'s equivalent to energies within the band gap of the semiconductor and under conditions where the band edges remain fixed with respect to solution levels, the electron-transfer reaction occurs with the semiconductor in the depletion region. Under these conditions, variations of E mainly affect p_{so} and produce an α of one. Alternatively, for couples that lie below the valence band of a p-type semiconductor, the electron transfer occurs with the semiconductor in the accumulation region. As the semiconductor surface becomes degenerate, p_{so} tends to a large constant value and the behavior approaches

that of the metal/solution interface, where variations of k_{et} with E and $\alpha \approx 0.5$ prevail. In previous studies of numerous couples located within the band gap, to our knowledge, only a few showed apparent transfer coefficients of 1, as expected for an ideal semiconductor/electrolyte interface,[7,8,14b,18-20] and only one reported kinetic currents showing the expected proportionality with the concentration of the redox couple in solution (reduction of ferricyanide on n-ZnO).[7] The lack of agreement between experimental $i–E$ results and theory has been ascribed to the difficulties encountered in making such measurements with standard electrochemical techniques. Interpretation of the data is often complicated by the existence of parallel processes at the semiconductor surface, such as corrosion, which can contribute significantly to the measured current and also by the increased series resistance due to the semiconductor electrode itself. Any attempt to use low concentrations of redox couples to avoid uncompensated resistance problems is likely to be thwarted by an increase in the contribution of corrosion to the measured current. While transient measurements of kinetics have been reported,[16] charging current and resistance effects complicate the data analysis, so that most of the studies have used steady-state techniques, such as the rotating disk electrode[14] or the wall-jet electrode.[12] Although rotating disk voltammetry is widely used in studies with metal electrodes, it is often difficult to fabricate disk electrodes from many semiconductors, e.g., p-WSe₂.[14] Reliable kinetic data has been obtained for ferrocene derivatives in acetonitrile at WSe₂ using a wall-jet cell design; however, the method requires relatively large, defect-free crystals.[14] Progress has been made by the construction of a cell which allows electrochemical measurements to be made in millimeter-sized drops of electrolyte placed on a region of the WSe₂ crystal that is free of visible defects.[21]

Some of these problems can also be avoided by using the scanning capability of SECM. The tip can be used to generate a high local concentration of mediator, e.g., ferrocenium, at a
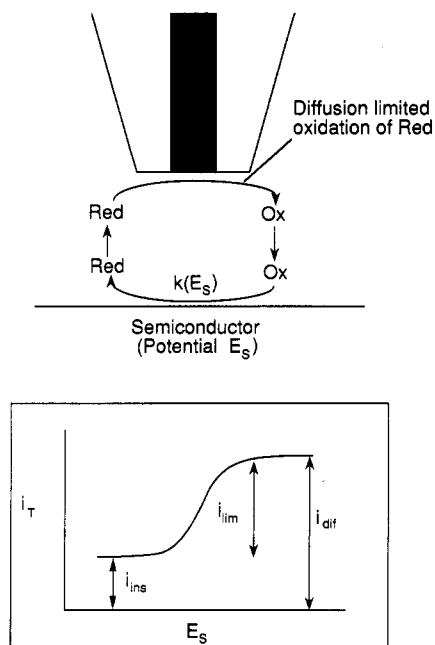
Figure 1. Schematic of the feedback method of measuring heterogeneous kinetics at semiconductors. The tip is poised at a potential where Red is oxidized at the diffusion-controlled rate; the flux of Red back from the surface and hence the tip current, i_T, depends on the rate of reduction at the semiconductor surface. The i_T–E_S curve has the form of an irreversible steady-state voltammogram.

specific point on a semiconductor crystal underneath the tip. The diffusion-limited tip current then depends on the rate of regeneration of ferrocene at the semiconductor (Figure 1). When the semiconductor is poised at a potential where the reduction is slow due to the presence of a depletion layer, the only effect of the semiconductor is to block diffusion to the tip, and the current due to diffusion of ferrocene into the gap (i_{ins}) is given by the same expression derived previously for an insulating substrate.[22] However, when the potential of the semiconductor is sufficiently negative that ferrocenium is reduced at a diffusion-controlled rate at the semiconductor, the tip current (i_{dif}) is given by the same expression derived for diffusion-controlled reactions at metal substrates.[22] At intermediate potentials, the tip current depends on the rate of heterogeneous electron transfer at the semiconductor and the rate of diffusion of ferrocene in the tip–substrate gap. As the semiconductor potential is swept more negative, the tip current increases from i_{ins} to i_{dif} and a plot of tip current versus substrate potential (i_T vs E_S) will have the form of a steady-state voltammogram with an offset at positive potentials of i_{ins}. The analysis of this type of voltammogram is discussed in the section on experimental procedure. This type of experiment has the advantages of ultramicroelectrode (UME) measurements without the need to construct a microelectrode from the semiconductor itself. Furthermore, when the tip-to-surface distance is less than the tip radius, thin-layer cell behavior is observed.[23] This allows the use of the simple theory for steady-state voltammetry at uniformly accessible electrodes and the determination of reliable values of rate constants and transfer coefficients for fast reactions.[23] This type of measurement is free of problems associated with uncompensated solution resistance because of the low (typically nanoamps) currents involved. The technique is also less sensitive to the existence of parallel reactions as long as these processes do not produce soluble electroactive species which can contribute to the tip current or interfere with the charge-transfer process at the semiconductor itself, e.g., by forming a passivating oxide layer.

In this work, we describe the measurement of the heterogeneous electron-transfer kinetics for electron transfer from n-WSe₂, p-WSe₂, and n-Si to several outer-sphere redox couples. The results are compared with the predictions of standard theories of electron transfer at semiconductor/liquid interfaces.[8,24–31]

Experimental Section

Chemicals. Acetonitrile (MeCN) (Burdick and Jackson, UV grade, 0.004% water) and methanol (MeOH) (Mallinkrodt, Paris, KY) were dried over neutral alumina (ICN Biomedicals, Germany) when necessary. Lithium perchlorate was used as received. Ru(NH₃)₆²⁺ was prepared by reduction of a solution of Ru(NH₃)₆Cl₃ (Strem Chemicals Inc., Newburyport, MA) over amalgamated zinc in the SECM glovebox and then added directly to the cell. All other redox couples and chemicals were obtained from Aldrich (Milwaukee, WI). Ferrocene and N,N,N′,N′-tetramethyl-1,4-phenylenediamine (TMPD) were purified by sublimation under vacuum in the usual manner.

Semiconductor Electrodes. n-WSe₂ and p-WSe₂ crystals were grown by the vapor transport method.[32] Fresh surfaces were prepared by peeling off the surface layers with adhesive tape. Ohmic contact was made by placing the crystal on a drop of silver paint (Acme Chemicals & Insulation Co., Allied Products Corp., New Haven, CT) on a glass disk. The electrical lead wire was then pushed into the silver paint, and the assembly was allowed to dry for about 2 h. A drop of 5-min epoxy was placed over the electrical lead and the crystal was covered with a hydrophobic lacquer (Micro Products, Hope, AR), leaving only the smooth van der Waals surface of the crystal exposed to solution. The geometric area of the exposed surface was determined by examining the electrodes under an optical microscope.

n-Si ({100} face, 1 Ω cm, Texas Instruments, Dallas, TX) electrodes were prepared in a similar way to WSe₂. Ohmic contacts were made by scratching part of the crystal with emery paper and rubbing with In–Ga alloy. The crystal was painted with a hydrophobic lacquer so that only the (100) surface was in contact with the electrolyte. The electrode was etched with 25% HF for several minutes and rinsed with dry MeCN or MeOH before each experiment.

Ultramicroelectrodes. SECM tips were prepared by sealing platinum wire (2-, 5-, 10-, or 25-μm diameter, Goodfellow Metals Ltd., Cambridge, U.K.) or carbon fibers (11-μm diameter, Amoco Performance Products, Greenville, SC) in glass as described previously.[22] The ratio of glass insulator to metal diameter at the tip (denoted RG) was 2–5. The tips were polished with 0.05-μm alumina (Buehler, Lake Bluff, IL) before each experiment, and their performance was checked by recording a voltammogram of the redox couple in the bulk solution.

Instrumentation. Most experiments were performed on the SECM described in ref 33; however, in cases where rigorous exclusion of oxygen was necessary (i.e., when solutions of Ru(NH₃)₆²⁺ were used), the glovebox SECM described in ref 34 was preferred. The semiconductor electrodes were placed on the bottom of a Teflon SECM cell described previously,[35] and the SECM was covered with black cloth to avoid photoexcitation of the semiconductor electrode. The reference electrode was either a Ag wire or an SCE. All potentials for experiments in aqueous solution reported here have been referred to an SCE reference. Potentials in MeCN are reported versus the formal potential of ferrocene. Voltammograms and current vs distance curves were obtained with an EI-400 bipotentiostat (Ensman Instruments, Bloomington, IN) or a BAS-100A electrochemical analyzer (Bioanalytical Systems, West Lafayette, IN).

Impedance data were obtained using a lock-in amplifier (Model 5210, EG&G Princeton Applied Research, Princeton, NJ) in combination with the EI-400 bipotentiostat or using the phase selective ac voltammetry option of the BAS-100A analyzer.

Theory

A brief discussion of the theories of electron transfer at semiconductor electrodes is given in order to clarify the terminol-

ogy used to discuss the results. The standard theories of electron transfer at semiconductor/liquid interfaces due to Marcus, Gerischer, and Morrison have been summarized in a recent review.[24] The current at a semiconductor electrode in the dark is given by eq 1. Theoretical expressions for k_{et} usually differ only in the preexponential factor. A familiar form for k_{et} is given in eq 2

$$k_{et} = k_{et}^0 \exp\left(-\frac{[\lambda + \Delta G^{0\prime}]^2}{4\lambda kT}\right) \quad (2)$$

where λ is the reorganization energy, k_{et}^0 is a preexponential factor, which depends on the distance over which electron transfer occurs and the appropriate frequency factor, and $\Delta G^{0\prime}$ (in eV) is the driving force for the reaction. $\Delta G^{0\prime}$ is equal to the difference between the formal potential of the redox couple and the energy of the valence band edge (for oxidation via the valence band of a p-type semiconductor). In the recent treatment by Gerischer,[31] k_{et}^0 is given by

$$k_{et}^0 = (2\pi/3)\nu_n\delta[r_e^3]\kappa_e \quad (3)$$

where ν_n is the nuclear frequency factor ($\approx 10^{13}$ s^{-1}), δ is the distance over which electron transfer occurs ($\approx 3 \times 10^{-8}$ cm), r_e is the radius of the electron wave function in the semiconductor ($\approx 10^{-7}$ cm),[32] and κ_e depends on the electronic interaction between the electron in the solid and the redox species, taken to be 1 in this work. With these estimates, the value of k_{et}^0 is estimated to be, very roughly, 6×10^{-16} cm^4 s^{-1}.[24]

The value of k_{et} is not measured directly but is related to the standard electrochemical rate constant k° (cm s^{-1}) by eq 4

$$k^\circ = k_{et}p^\circ_{so} \quad (4)$$

where p°_{so} is the surface hole concentration at the standard potential of the redox couple, p_{so} (at any potential) can be calculated from eq 5:

$$p_{so} = N \exp(FE_{sc}/RT) \quad (5)$$

where N is the dopant (acceptor) concentration and E_{sc} is the potential drop in the space charge region of the semiconductor. E_{sc} can be determined from impedance measurements when the band edges are fixed at the interface and all the applied potential appears across the space charge region.[12] For a semiconductor in the depletion region, the electrode potential only appears in the rate expressions through the hole concentration in eq 5, and theory predicts an apparent transfer coefficient of 1. The experimental results should also show no dependence of the rate constant on concentration of the redox couple.

Experimental Procedure and Data Analysis

The general procedure for all the experiments was to acquire a tip voltammogram (i_T vs E_T) of the redox couple with the tip far from the semiconductor surface. The tip was then adjusted to a potential on the diffusion-controlled plateau of the tip voltammogram and pushed toward the semiconductor surface. The tip was then scanned over the surface and an SECM image observed to find a smooth (on the micrometer scale) part of the crystal which was free from obvious defects. Current–distance (i_T–d) curves were recorded with the semiconductor at potentials where no regeneration of the redox mediator occurred (i.e., where the irreversible nature of the semiconductor electrode reaction produces no current at a p-type material at sufficiently negative potential and where the semiconductor thus behaves as an insulator for SECM purposes) and, if possible, where the regeneration was diffusion-controlled. Use of previous theory enables the absolute tip-to-surface distance to be extracted from either of these

measurements.[22,23] For an n-type semiconductor, insulator behavior was found with the semiconductor at sufficiently positive potentials. Next, the potential of the semiconductor was swept between the potential limits where there was no regeneration of the redox mediator at the semiconductor and where the regeneration was diffusion-controlled, with the tip still poised at a potential where the reaction at the tip is diffusion-controlled. A steady-state voltammogram of tip current vs semiconductor electrode potential was acquired with the PC of the SECM as described previously.[33] The voltammograms were analyzed by decomposing the total tip current, i_T, into the sum of the currents due to diffusion into the gap, i_{ins}, and the feedback current due to regeneration of the mediator at the semiconductor, i_{fdbk}:

$$i_T = i_{ins} + i_{fdbk} \quad (6)$$

The (small) current due to diffusion into the gap, i_{ins}, was approximated by the current at a potential where the semiconductor is effectively an insulator (see Figure 1). The current through the substrate, i_S, is then equal to the fraction of the tip current due to regeneration of the mediator and is given by

$$i_S = i_{fdbk} \quad (7)$$

We estimate that this introduces an error of 10–20% for typical tip–substrate separations; however, this is well within the scatter of the experimental values of the rate constants measured. At close tip–substrate separations, the current distribution is uniform and the effective area of the substrate is equal to the tip area, A. The mass-transport rate at the semiconductor, m_0, can then be calculated from

$$nFAcm_0 = i_{dif} - i_{ins} \quad (8)$$

where c is the concentration of the redox couple. The voltammograms (i_T vs E_S) were therefore analyzed by substracting i_{ins} (i.e., the tip current at potentials, E_S, where the semiconductor behaved as an insulator in SECM), and fitting the data to the general theoretical steady-state voltammograms for a completely irreversible electron transfer at uniformly accessible electrodes:[23]

$$i = nFAcm_0/(1 + m_0/k) \quad (9)$$

where k is the electrochemical (heterogeneous electron transfer) rate constant which, assuming Butler–Volmer kinetics, is related to potential via

$$k = k^\circ \exp[\alpha nF(E - E^{\circ\prime})/RT] \quad (10)$$

where α is the transfer coefficient and $E^{\circ\prime}$ is the formal potential of the redox couple.

Results

Heterogeneous Electron-Transfer Rate at the van der Waals Surface of Tungsten Diselenide/Ru(NH$_3$)$_6^{2+}$. In view of the resistance of layered semiconductors to corrosion and the possibility of preparing smooth surfaces by peeling off the surface layers, we chose WSe$_2$ for our initial studies.[36] The potentials of the band edges and doping densities of our n- and p-WSe$_2$, as obtained from plots of $1/c_{sc}^2$ vs E (Mott–Schottky plots, where c_{sc} is the space charge capacity), are given in Table 1, and the cases of p-WSe$_2$/0.5 M Na$_2$SO$_4$ and n-Si/MeCN are illustrated in Figure 2. A value of 12.5 was used for the dielectric constant[37] of WSe$_2$, and a value of 8.8×10^{18} cm^{-3} was used for the density of states at the bottom of the conduction band.[38] Following Koval and Olson,[12] the valence band density of states was assumed to be the same. Linear Mott–Schottky plots over a range of about 600–700 mV for n-type WSe$_2$ and 400 mV (0.25–0.65 V vs SCE) for p-type WSe$_2$ were obtained. There was no significant

TABLE 1: Flatband Potentials, Band Edge Positions, and Doping Densities for n-WSe$_2$/0.1 M KCl and p-WSe$_2$/0.5 M Na$_2$SO$_4$

	p-WSe$_2$/0.5 M Na$_2$SO$_4$	n-WSe$_2$/0.1 M KCl
E_{fb} (V vs SCE)	+0.66	−0.36
doping density (cm^{-3})	4 × 10^{15}	2 × 10^{16}
dielectric constant	12.5	12.5
N_c or N_v (cm^{-3})	8.8 × 10^{18}	8.8 × 10^{18}
E_v (V vs SCE)	+0.86	+0.85[a]
E_c (V vs SCE)	−0.51[a]	−0.52

[a] Assuming a band gap of 1.37 eV.[51]
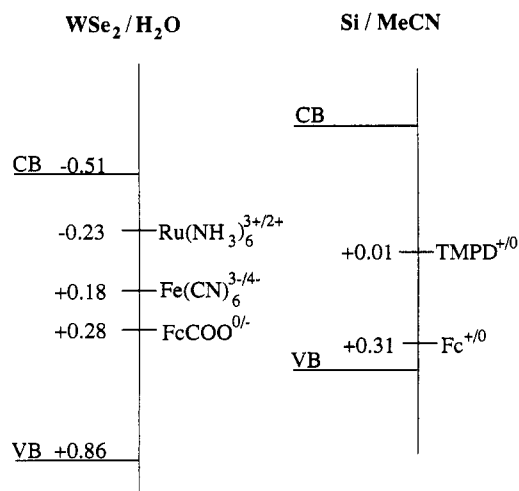
Figure 2. Formal potentials and band edge positions of the redox couples and semiconductors studied. All the potentials are given vs SCE. The band edge positions for silicon are not known, but the conduction band edge is estimated to be approximately −0.8 V vs SCE.[5]
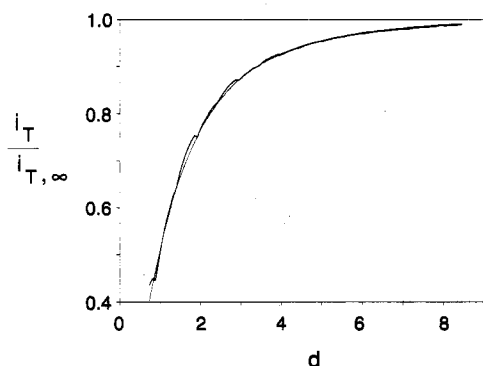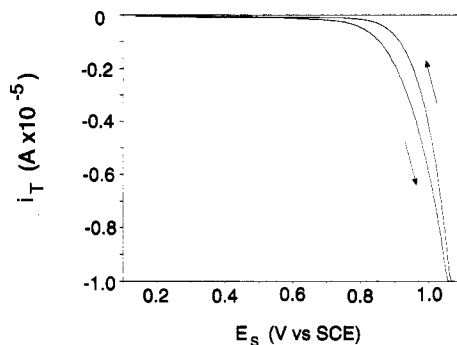

Figure 3. An approach curve for a 10-μm-diameter Pt tip reducing Ru(NH$_3$)$_6$$^{3+}$ (4.78 mM) in 0.5 M Na$_2$SO$_4$. The potential of the p-WSe$_2$ substrate was +0.4 V, where oxidation of the Ru(NH$_3$)$_6$$^{2+}$ does not occur. The bold line is the experimental data, and the thin line is theory.

frequency dispersion in the range 200 Hz to 1 kHz. A value of −0.23 V vs SCE was determined for the formal potential of Ru(NH$_3$)$_6$$^{3+/2+}$ in Na$_2$SO$_4$ by steady-state voltammetry at a 25-μm-diameter platinum UME.

Figure 3 shows a typical approach curve with the semiconductor in the "insulator region" used to determine the tip–surface distance and the mass-transport rate from eq 8. Figure 4A shows a typical tip current–substrate potential (i_T–E_S) voltammogram for the oxidation of Ru(NH$_3$)$_6$$^{2+}$ on p-WSe$_2$. The bulk solution contained 4.78 mM Ru(NH$_3$)$_6$Cl$_3$ in 0.5 M Na$_2$SO$_4$ and the tip was 10-μm-diameter platinum. Figure 4B shows the fit to theory for the forward scan, after subtracting the small current at the negative end of the potential range due to the diffusion of Ru(NH$_3$)$_6$$^{2+}$ into the tip–substrate gap (i_{ins}). Near the limiting current, the slope of the voltammogram deviates from theory, but the fit is good up to about +0.65 V. Figure 5 shows a typical current–voltage scan of the semiconductor itself; this current is small over the region of interest, indicating that uncompensated resistance

Figure 4. Kinetic voltammograms (i_T–E_S) for the oxidation of Ru(NH$_3$)$_6$$^{2+}$ on p-WSe$_2$ in 0.5 M Na$_2$SO$_4$. The tip was 10-μm-diameter platinum, and the concentration of Ru(NH$_3$)$_6$$^{3+}$ in the bulk solution was 4.78 mM. (A) Raw data. (B) Fitted voltammogram (bold line is experiment).
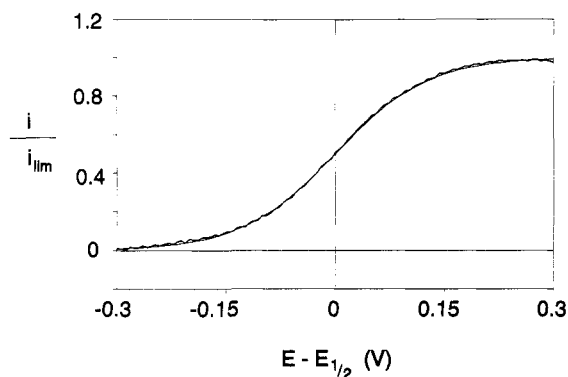

Figure 5. A typical current–voltage curve for the p-WSe$_2$ substrate in background electrolyte (0.1 M KCl). No significant difference was observed in 0.5 M Na$_2$SO$_4$.

in the semiconductor is not the cause of the deviation from theory at potentials greater than 0.65 V. The reason for the deviation at positive potentials could be movement of the band edges in the semiconductor as the bands flatten, causing a decrease in the transfer coefficient. However, the lack of retraceability of the original data at potentials greater than 0.65 V may also indicate that a slow change in the surface is occurring (e.g., the onset of anodic corrosion), and the data in this potential region were therefore not analyzed in detail. However, the i–E curve (Figure 4A) does retrace in the region where the electron-transfer rate was calculated, showing that the surface is not irreversibly damaged. The kinetic parameters obtained by fitting voltammograms of Ru(NH$_3$)$_6$$^{2+}$ at p-WSe$_2$/0.5 M Na$_2$SO$_4$ with a range of concentrations and mass-transport rates (different tip–substrate separations) are collected in Table 2. All the voltammograms fit the theory for an irreversible reaction with a formal transfer coefficient, α, of 1.0 ± 0.05. This is as expected for a simple outer-sphere reaction at a semiconductor in depletion. The standard heterogeneous rate constant, $k°$, extrapolated to the formal potential of Ru(NH$_3$)$_6$$^{2+/3+}$ was (1.7 ± 0.6) × 10^{-16} cm s^{-1}. Note that this value was independent of concentration and

TABLE 2: Kinetic Data for the Oxidation of Ru(NH₃)₆²⁺ on p-WSe₂/0.5 M Na₂SO₄

[Ru(NH₃)₆³⁺] (mM)	m_0 (cm s⁻¹)	$E_{1/2} - E^{\circ\prime}$ (V)	k° (10⁻¹⁶ cm s⁻¹)	k_{et} (10⁻¹⁷ cm⁴ s⁻¹)
4.8	0.038	0.846	1.9	6.5
4.8	0.046	0.850	1.9	6.6
4.8	0.046	0.852	1.8	6.1
4.8	0.046	0.850	1.9	6.6
4.8	0.042	0.858	1.3	4.4
4.8	0.023	0.831	2.0	6.9
4.8	0.019	0.825	2.1	7.2
2.8	0.046	0.861	1.3	4.3
2.8	0.046	0.862	1.2	4.2
1.7	0.048	0.855	1.7	5.7
1.7	0.048	0.855	1.7	5.7
1.0	0.049	0.859	1.4	4.9
1.0	0.051	0.855	1.8	6.0
1.0	0.050	0.859	1.5	5.1
			1.7 ± 0.6ᵃ	5.7 ± 1.0ᵃ

ᵃ Mean value.

Figure 6. Theoretical and experimental voltammograms (i_T–E_S) for the oxidation of Ru(NH₃)₆²⁺ on p-WSe₂ in 0.1 M KCl. The tip was 10-μm-diameter platinum. The bold line is experimental data and the thin line is theory. [Ru(HN₃)₆³⁺] = 1.68 mM.

mass-transport rate within experimental error. From the data in Table 1 and a hole concentration at the electrode surface calculated from eq 5, we obtain a value of k_{et} = (5.7 ± 1.0) × 10⁻¹⁷ cm⁴ s⁻¹ (where k_{et} is the rate constant considering the process as a bimolecular reaction between holes and Ru(NH₃)₆²⁺). If the preexponential factor is taken to be of order 6 × 10⁻¹⁶ cm⁴ s⁻¹ (see above), a reasonable value of approximately 0.7 eV for the reorganization energy is obtained. The kinetic data for this reaction appear to be in agreement with the predictions of theory; however, the reorganization energy is not sensitive to the exact value of the rate constant and should only be taken as a rough estimate. Because Cl⁻ was introduced as the counterion (as Ru(NH₃)₆Cl₃), and Cl⁻ was shown to affect the behavior of the p-WSe₂ electrode at higher concentrations, experiments were not performed at Ru(NH₃)₆³⁺ concentrations above 5 mM (i.e., 15 mM Cl⁻). For reasons which are not clear, the apparent transfer coefficient in 0.1 M KCl is significantly lower than in 0.5 M Na₂SO₄ (~0.4). Figure 6 shows a i_T–E_S voltammogram in KCl obtained on the same p-WSe₂ crystal as used in the experiments yielding Figure 4. No difference in flat band potential was observed between these two electrolytes.

Surface Scans at p-WSe₂/Ru(NH₃)₆²⁺. The SECM can be employed to distinguish locations of different reactivity, e.g., different heterogeneous reaction rates, on a surface (SECM reaction rate imaging),[39] and we have used this approach to observe variations in the electron-transfer rate with Ru(NH₃)₆²⁺ on p-WSe₂ in Cl⁻ solutions. By using a 2-μm-diameter tip and carefully scanning across the surface, we could observe different kinetic behavior at different sites on the surface. Figure 7 shows several SECM line scans across the same region of a p-WSe₂ surface in 0.1 M KCl with the tip reducing Ru(NH₃)₆³⁺ at the diffusion-controlled rate and the semiconductor biased at different
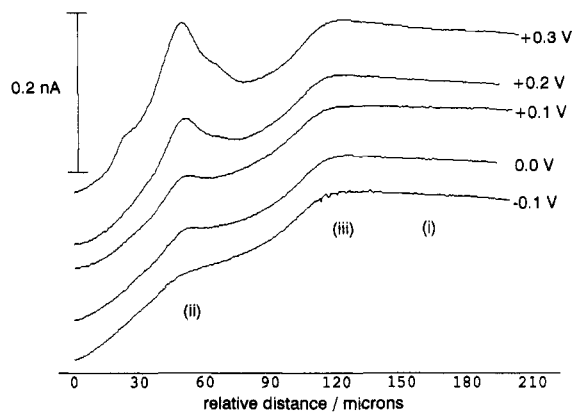
Figure 7. SECM line scans across a stepped portion of a p-WSe₂ surface in 0.1 M KCl, with the tip poised at a potential on the diffusion-controlled plateau of Ru(NH₃)₆³⁺ (4.39 mM) reduction. The tip was 2-μm-diameter platinum and $i_{T,\infty}$ was ca. 1.5 nA. The potential of the semiconductor substrate (vs SCE) is indicated on the right of each line scan. For clarity, the curves have been offset by approximately 50 pA.
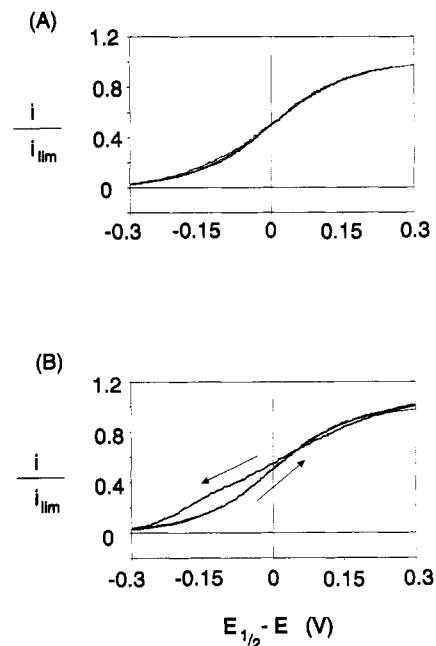
potentials positive of the formal potential of Ru(NH₃)₆²⁺/³⁺ but less than the flatband potential of p-WSe₂. The curve at –0.1 V, where the semiconductor acts purely as an insulator, reflects the surface topography and shows two steps (both roughly 0.5 μm in height) on the left of the figure. Low currents imply close tip–surface separations so the bottom of the steps is on the right of the figure. As the semiconductor potential is increased, current peaks grow in at 60 and 120 μm at the steps. Figure 8A,B,C shows i_T–E_S voltammograms taken at positions i, ii, and iii of Figure 7. At position i (Figure 8A), on the flat (basal plane) part of the surface, the voltammogram could be fit with a transfer coefficient of 1 in this electrolyte. This voltammogram, however, indicates two limitations of the technique. The very high mass-transport rate at the small tip causes a displacement of the voltammogram to positive potentials, and a complete voltammogram was not obtained to avoid increasing the positive potential limit to values where corrosion of the WSe₂ surface occurs. Moreover, the current due to diffusion of mediator into the tip–substrate gap (i_{ins}) dominates the kinetic current at potentials ≲0.6 V. Nevertheless, the voltammogram shape at this site shows ideal behavior (i.e., $\alpha \approx 1$) despite the presence of defects on the surface which contribute significantly to the overall substrate current (Figure 8D). In contrast, near the step edge at position ii (Figure 8B), the i_T–E_S voltammogram is much less steep and already shows a significant feedback current at 0.3 V. Near the step edge at position iii (Figure 8C), the i_T–E_S voltammogram shows intermediate behavior, rising sharply at about 0.5 V but then plateauing at a current too small to be diffusion-controlled. All these results can be rationalized by assuming that the step edges are associated with states in the band gap which provide facile paths for electron transfer to redox couples in the electrolyte and for anodic corrosion.[40–42] The difference between the behavior in parts B and C of Figure 8 might be due to the presence of corrosion products at position iii, e.g., tungsten oxides. The apparent effect of KCl electrolyte in the data obtained with a large tip may therefore reflect an enhancement of the kinetics of Ru(NH₃)₆²⁺ oxidation at the step sites perhaps due to adsorption of chloride on the tungsten atoms exposed at the step edges and a *local* shift of the flat band to more negative potentials. The unique ability of the SECM to obtain i–E curves and probe reaction rates on sites of micrometer-level dimensions may be useful in probing the effect of surface defects on electron-transfer kinetics.

Heterogeneous Kinetics for WSe₂ and Other Redox Species. Despite the satisfactory (though rough) agreement with theoretical predictions, the oxidation of Ru(NH₃)₆²⁺ was unique, and all other couples we studied showed different behavior. Table 3 shows the half-wave potentials and transfer coefficients for various

(A)

(B)

(C)

(D)
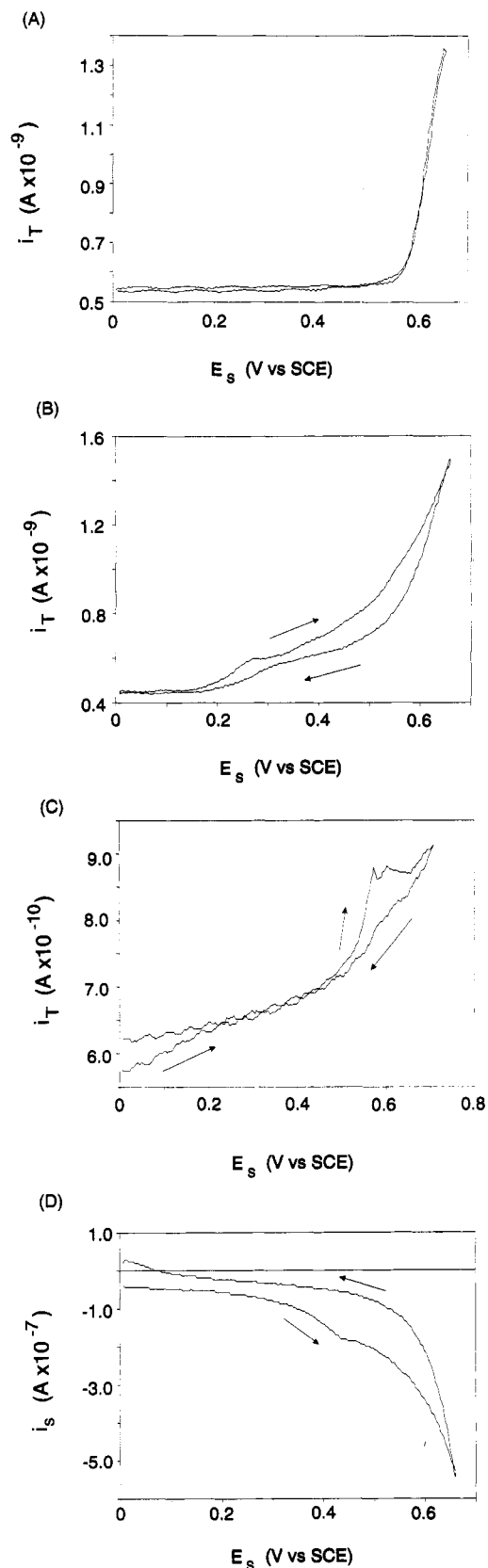
Figure 8. Kinetic voltammograms (i_T–E_S) obtained on placing the tip close to the semiconductor surface at points i, ii, and iii indicated in Figure 7. (A) i, (B) ii, (C) iii, and (D) substrate current during A–C.

(A)

(B)

Figure 9. Theoretical fits and experimental voltammograms for the reduction of $Ru(NH_3)_6^{3+}$ on n-WSe₂ in 0.1 M KCl. $[Ru(HN_3)_6^{2+}]$ = 1.08 mM. 11-μm-diameter C fiber tip. The bold lines are experimental data. Sweep rate, (A) 100 mV s⁻¹ and (B) 10 mV s⁻¹.

redox couples on n- and p-WSe₂. The low transfer coefficient for ferrocyanide may arise because the half-wave potential for this couple is more positive than that for $Ru(NH_3)_6^{3+/2+}$. Here the oxidation occurs at potentials more positive than the flatband potential (0.66 V), where the semiconductor becomes degenerate and would be expected to show a transfer coefficient of ~0.5 as

commonly observed on metals.[43] The reason for the more positive half-wave potential is not clear, but may simply reflect the slower inherent kinetics of this couple, although Memming and co-workers have claimed very fast kinetics for this reaction at pH 0.[14] No attempt to analyze this case in detail was made because at these positive potentials anodic corrosion of the semiconductor occurs (Figure 5).

For the reduction of sodium ferrocenium carboxylate on n-WSe₂, a well-defined voltammogram was not obtained. Instead, the i_T–E_S curve showed a linear ln i vs E plot with an apparent transfer coefficient of about 0.1. Anomalously low transfer coefficients of this order were also observed by Koval and co-workers for the reduction of Fe^{3+}, $FeCN_6^{3-}$, and $Co(phen)_3^{3+}$ on n-WSe₂ in 1 M HClO₄.[11] These authors attributed this low value to a tunneling process to the valence band as the band edges of the semiconductor shift more negative with increasing accumulation. The transfer coefficient of 0.3 for the reduction of $Ru(NH_3)_6^{3+}$ is lower than that observed by Koval and co-workers (who reported a slope of 130 mV dec⁻¹ or α = 0.45).[11] Figure 9 shows the data for this system at different sweep rates. The appearance of hysteresis at low sweep rates when the negative potential limit is beyond $E_{1/2}$ suggests a slow surface process occurs at negative potentials. Although the reduction of $Ru(NH_3)_6^{3+}$ occurs before evolution of hydrogen commences, intercalation of H atoms can occur at more negative potentials;[44] this may contribute to the nonideal behavior of this interface. Thus, at least in this electrolyte, 0.1 M KCl, the WSe₂ surface does not appear to be well-behaved. Note that the transfer coefficients (α) shown in Table 3 are significantly less than 0.5 for a variety of different systems. The data of Koval and Olson for ferrocene derivatives at n-WSe₂ in acetonitrile also yields similar values of transfer coefficients.[12] We can rule out resistance effects as the explanation for the small α values, because the currents through the semiconductor in our experiments are small (of the order of 100 nA or less). The iR drop would therefore be only a few millivolts even for resistances of the order of 10 kΩ, which is much greater than is attributable to the solution or the semiconductor. On the basis of the observations of different kinetics at different locations on the surface (Figure 8), we tentatively suggest that the low apparent transfer coefficients found in many experiments with macroscopic samples of a
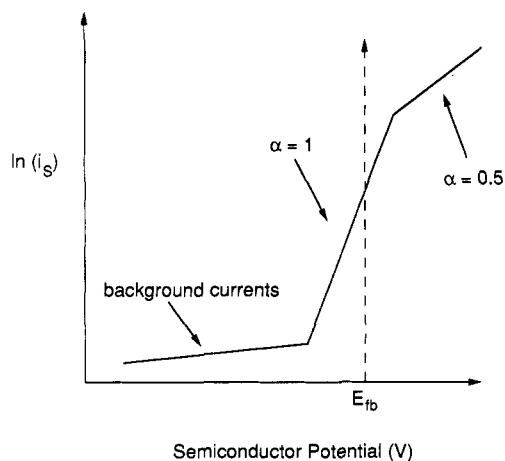
Figure 10. Schematic diagram showing the variation of the electron-transfer rate and transfer coefficient (α) with potential for a semiconductor–liquid interface.

semiconductor are the result of averaging the kinetics over a distribution of sites with different local kinetics, in the same manner proposed by Finklea and co-workers, who observed low transfer coefficients at gold electrodes coated with monolayers of alkanethiols.[45]

No examples of $\alpha = 1$ were found for reduction on n-WSe$_2$, even though oxidative corrosion of the semiconductor does not occur under these conditions. The reason for this is uncertain, but may simply reflect the severe constraints for obtaining ideal behavior. In addition to the necessity for stability of the band edge position with change in potential and rapid kinetics of the redox couple, ideal behavior is only expected over a fairly narrow potential region. Far from flatband, in depletion, the concentration of majority carriers at the surface is very low, and the current is probably dominated by artifacts and parallel pathways via surface states. When the potential passes through flatband, the semiconductor eventually becomes degenerate and the band edges are no longer fixed. In this situation, the semiconductor behaves as a metal and a value of 0.5 is expected for the transfer coefficient (Figure 10). Therefore, only a narrow potential window around the flatband is available where the concentration of majority carriers at the surface follows eq 5 and the current is measurable.

Kinetics at the Silicon/MeCN Interface. No examples of $\alpha = 1$ were found for dark reductions on n-Si. Figure 11 shows the i_T–E_S voltammograms for the tip oxidation of ferrocene and TMPD in MeCN. Initially, the silicon was poised at –1 V to protect the surface against oxidation. Considerable hysteresis was observed between the forward (positive going) and backward scans. An apparent transfer coefficient of 0.29 for both couples was observed on fitting the forward scan (Figure 12 and Table 3). Repeatedly cycling the silicon removed the hysteresis, but the voltammogram became more drawn out ($\alpha \approx 0.2$). Chazaviel has shown that the Si/MeCN interface is not stable and that shifts of the flatband and the appearance of OH stretches in the infrared spectrum occur with time.[46] A plausible explanation for the decrease of the transfer coefficient is that an oxide layer, through which electrons must tunnel, is built up on exposing the electrode to anodic potentials because of reaction of Si with trace water or oxygen. The reason for the low initial value of α is not clear; however, the similarity of the results for the two redox couples suggests that it is a property of the Si/MeCN interface and is not specific to the redox couple.

In view of the excellent performance of n-Si/MeOH photo-electrochemical cells for solar energy conversion[47–49] and the reported stability of the band edges in Kelvin probe and impedance measurements,[46] we decided to investigate the behavior of the same redox couples in MeOH. Although stable, reproducible voltammograms were obtained for the oxidation of TMPD in MeOH, a noticeable hysteresis between forward and reverse scans
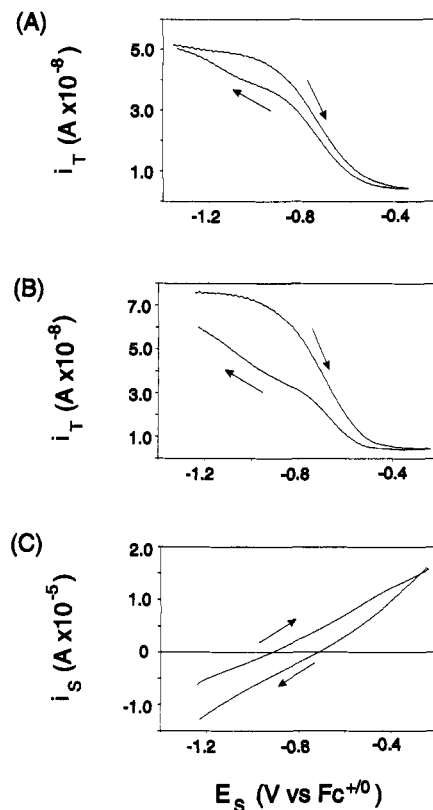
Figure 11. Voltammograms (i_T–E_S) for the reduction of (A) TMPD$^{\bullet+}$ and (B) ferrocenium on n-Si in acetonitrile. The tip was 10-μm-diameter platinum and the electrolyte was 0.3 M in LiClO$_4$. The bulk concentrations of TMPD and ferrocene were 8.52 and 2.15 mM, respectively. The current through the n-Si substrate for the ferrocene case is shown in (C).
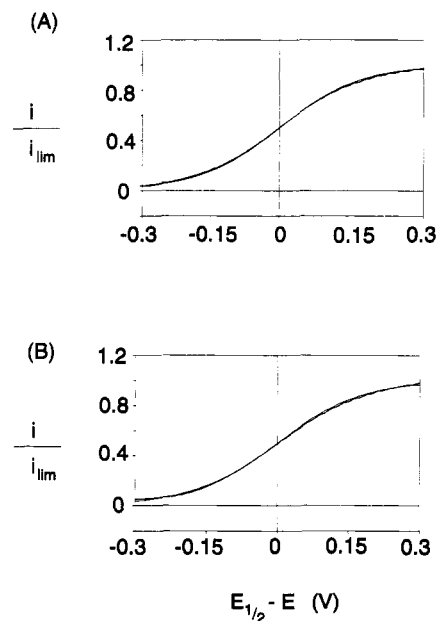
Figure 12. Theoretical fits for the data of Figure 11 and the values of α given in Table 3. Part A corresponds to Figure 11A (TMPD) and part B to Figure 11B (ferrocene). The bold lines are experimental data and the thin line is theory.

was still found (Figure 13). Although a larger transfer coefficient was observed in MeOH compared to this reaction in MeCN (Table 3), the value was still much lower than that expected for an ideal semiconductor/liquid interface in depletion.

In the case of ferrocene, the tip current was independent of substrate potential, even at n-Si potentials positive of the formal potential of the redox couple. This indicates that ferrocenium generated at the tip reacts chemically with the silicon surface.

TABLE 3: Kinetic Data for Various Outer-Sphere Redox Couples on WSe2 and Si

| electrolyte	substrate	couple	process	$E^{o\prime}$ (V vs SCE)	α
0.1 M KCl	n-WSe2	Ru(NH3)6	reduction	−0.19	0.3
0.5 M Na2SO4	p-WSe2	Ru(NH3)6	oxidation	−0.23	1.0
0.1 M KCl	p-WSe2	Ru(NH3)6	oxidation	−0.19	0.4[a]
0.1 M KCl	n-WSe2	FcCOONa	reduction	+0.28	0.1
0.5 M Na2SO4	p-WSe2	Fe(CN)6³⁻/⁴⁻	oxidation	+0.18	0.43
LiClO4/MeCN	n-Si	ferrocene	reduction	+0.31	0.29
LiClO4/MeCN	n-Si	TMPD	reduction	+0.01	0.29
LiClO4/MeOH	n-Si	TMPD	reduction	+0.01	0.62
LiClO4/MeOH	n-Si	ferrocene	reduction	reacts chemically	

[a] At a 10-μm tip; see text.
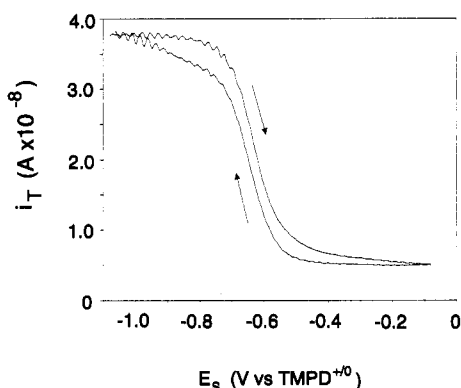
Figure 13. Raw data (i_T–E_S) for the reduction of TMPD$^{\bullet+}$ on n-Si in methanol. The tip was 10-μm-diameter platinum, and the electrolyte was 0.3 M in LiClO4. The concentration of TMPD in the bulk solution was 4.52 mM.
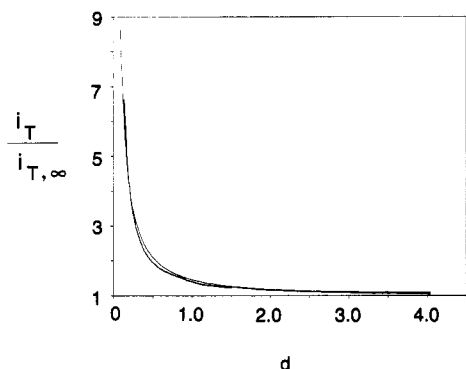

Figure 14. Theoretical and experimental approach curves (i_T–d) for a 5-μm-diameter platinum tip oxidizing ferrocene (4.57 mM) at the surface of unbiased n-Si. The theoretical line (thin line) was calculated for diffusion-controlled reduction of ferrocenium at the silicon. The bold line is experimental data, at the point of closest approach, the mass-transport rate is 0.37 cm s⁻¹.

The fact that ferrocenium can inject holes into the valence band of Si in MeOH but not in MeCN can be attributed to the band edges lying at more negative values in MeOH.[46,47] Figure 14 shows an approach curve over unbiased n-Si, where the curve fits the theory for diffusion-controlled regeneration of ferrocene. The mass-transport rate at the closest distance in Figure 14 is 0.37 cm s⁻¹, and this sets a lower bound on the heterogeneous rate constant for the reduction of ferrocenium at the silicon surface. In the case of GaAs,[50] previous work showed that injection of holes into n-type material resulted in etching because the holes localize at the surface and oxidation occurs. For Si, such hole injection might be expected to lead to rapid passivation by the formation of an oxide layer so that the current would decay below $i_{T,\infty}$; however, this was not observed. Instead, the current decayed only slightly over a period of about 15 min (Figure 15) and remained in the positive feedback region. After 15 min, the tip was scanned laterally across the surface and the resulting line
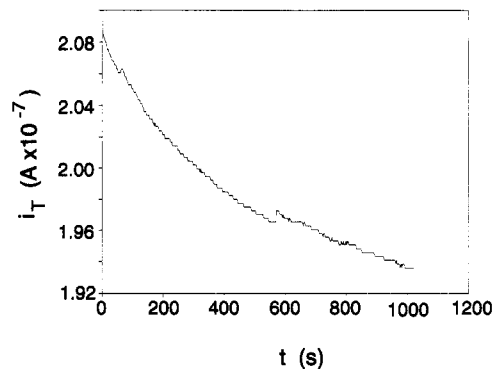
Figure 15. Tip current against time for a 25-μm-diameter platinum tip oxidizing ferrocene ca. 3 μm from an unbiased n-Si surface in 0.3 M LiClO4/MeOH; $i_{T,\infty}$ was 59 nA.
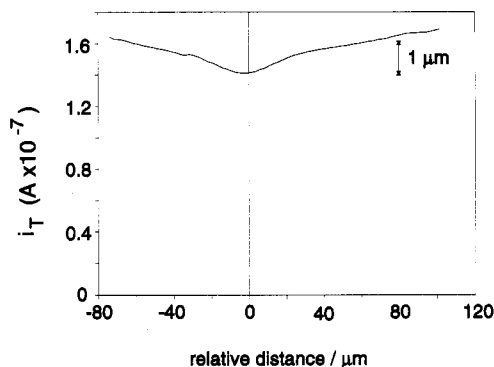
Figure 16. Line scan across an etched spot on an unbiased n-Si surface in 0.3 M LiClO4/MeOH. The etch spot was made by holding the tip close (ca. 3 μm) to the silicon surface for 15 min (Figure 15). The tip was then partially withdrawn and scanned horizontally across the surface to observe the local topography.

scan (Figure 16) showed a dip over the original position of the tip. Assuming this dip is caused by the presence of an etch pit, the depth of the pit is about 1 μm. Infrared spectroscopic data have shown that in methanol the surface is protected against passivation by methoxylation.[46] Perhaps the silicon is etched and Si^{IV} dissolves in the form of Si(OMe)4.

Conclusions

The oxidation of Ru(NH3)6²⁺ at p-WSe2/0.5 M Na2SO4 follows theory for an ideal semiconductor/liquid interface; i.e., the potential dependence of the current is determined entirely by the concentration of majority carriers at the surface and the band edges are fixed at the surface in the potential range where the reaction occurs. The magnitude of the rate constant is in rough agreement with the predictions of standard theories of electron transfer at semiconductor electrodes. To the best of our knowledge, this is the first example of ideal behavior for a dark process of an outer-sphere redox couple at a p-type semiconductor. By scanning with a small (2 μm) tip we were able to observe directly the different kinetic behavior on the van der Waals surface (apparent transfer coefficient = 1) and at step edges where the current is significant for the oxidation of Ru(bpy)3²⁺, even 0.4 V negative of the flatband potential, and rises more gradually with potential.

All other redox couples examined in this work on either WSe2/ aqueous or n-Si/MeOH or MeCN interfaces showed smaller transfer coefficients. In one case (FeCN6⁴⁻/³⁻ on p-WSe2), a transfer coefficient near 0.5 was observed, which is attributable to degeneracy of the semiconductor resulting in metal-like behavior. However, several systems (Fc, TMPD at n-Si/MeCN and Ru(NH3)6²⁺/³⁺ at n-WSe2) showed anomalously low transfer coefficients of about 0.3. We suggest that the explanation of Finklea and coworkers for reactions at alkanethiol-coated gold

electrodes[45] applies here too, namely, that the low transfer coefficients obtained from kinetic data at macroscopic electrodes is the result of an average over different microscopic sites of different reactivity.

In agreement with earlier reports, the behavior of n-Si in MeOH is very different to that in MeCN; the band edges are shifted more negative and the voltammograms are stable, indicating that the surface is also stable in this solvent. As suggested by Chazaviel,[46] the surface appears to be protected against passivation.

List of Symbols

α	formal transfer coefficient
A	geometric area of tip electrode
d	tip-to-surface distance normalized by the tip radius
c	concentration of redox couple
c_{sc}	space charge capacity
$E_{1/2}$	half-wave potential (V)
E_{fb}, E_c, E_v	flatband potential, conduction band edge, and valence band edge (V)
$E^{o\prime}$	formal potential of a redox couple
E_S	potential of substrate electrode (here, a semiconductor) (V)
E_{sc}	potential drop in space charge region of semiconductor (V)
i_{dif}	diffusion-limited tip current with positive feedback (A)
i_{fdbk}	feedback current at the tip due to regeneration of mediator (A)
i_{ins}	diffusion-limited tip current near an insulating surface (A)
i_{lim}	diffusion-limited current after background subtraction (A)
i_S	current through substrate (A)
i_T	tip current close to surface (A)
$i_{T,\infty}$	diffusion-controlled current at tip in bulk solution (A)
k	electrochemical heterogeneous electron-transfer rate constant
k_{et}	electrochemical rate constant normalized by hole concentration at surface $(cm^4 s^{-1})$; also bimolecular electron-transfer rate constant $(cm^4 s^{-1})$
k_{et}^0	preexponential factor
k^o	standard heterogeneous electrochemical rate constant $(cm\ s^{-1})$
λ	reorganization energy (eV)
m_0	mass-transport coefficient $(cm\ s^{-1})$
N	dopant (acceptor) concentration
N_v, N_c	valence band and conduction band densities of states (cm^{-3})
p_{so}	concentration of majority carriers at the surface (cm^{-3})
$p^o{}_{so}$	surface hole concentration at the standard potential of the redox couple

References and Notes

(1) Lewis, N. S. *Acc. Chem. Res.* **1990**, *23*, 176.

(2) Wrighton, M. S. *Acc. Chem. Res.* **1979**, *12*, 303.

(3) *Photoeffects at Semiconductor-Electrolyte Interfaces*; Nozik, A. J., Ed.; ACS Symposium Series 146; American Chemical Society: Washington, DC, 1981.

(4) Peter, L. M. In *Electrochemistry*; Pletcher, D., Ed.; Specialist Periodic Report; Royal Society of Chemistry: London, 1984; Vol. 9, p 66.

(5) *Semiconductor Electrodes*; Studies in Physical and Theoretical Chemistry; Finklea, H. O., Ed.; Elsevier: Amsterdam, 1988; Vol. 55.

(6) Memming, R. In *Topics in Current Chemistry*; Steckhan, E., Ed.; Springer-Verlag: New York, 1988; Vol. 143, p 79.

(7) Gerischer, H. In *Physical Chemistry: An Advanced Treatise*; Eyring, H., Ed.; Academic Press: New York, 1970; Vol. 9A (Electrochemistry), p 463.

(8) Morrison, S. R. *Electrochemistry at Semiconductor and Oxidized Metal Electrodes*; Plenum: New York, 1980.

(9) Freund, T.; Morrison, S. R. *Surf. Sci.* **1968**, *9*, 119.

(10) Koval, C. A.; Austermann, R. L.; Turner, J. A.; Parkinson, B. A. *J. Electrochem. Soc.* **1985**, *132*, 613.

(11) Koval, C. A.; Olson, J. B.; Parkinson, B. A. In *Electrochemical Surface Science: Molecular Phenomena at Electrode Surfaces*; Soriaga, M. P.; Ed.; ACS Symposium Series 378; American Chemical Society: Washington, DC, 1988; p 438.

(12) Koval, C. A.; Olson, J. B. *J. Phys. Chem.* **1988**, *92*, 6726.

(13) Frank, S. N.; Bard, A. J. *J. Am. Chem. Soc.* **1975**, *97*, 7427.

(14) (a) Sinn, C.; Meissner, D.; Memming, R. *J. Electrochem. Soc.* **1990**, *137*, 168. (b) Meissner, D.; Memming, R. *Electrochim. Acta* **1992**, *37*, 799.

(15) Mollers, F.; Memming, R. *Ber. Bunsen-Ges. Phys. Chem.* **1972**, *76*, 475.

(16) Nakabayashi, S.; Itoh, K.; Fujishima, A.; Honda, K. *J. Phys. Chem.* **1983**, *87*, 3487.

(17) Ahmed, S. M.; Gerischer, G. *Electrochim. Acta* **1979**, *24*, 705.

(18) Anodic corrosion of p-GaAs in H_2SO_4 (aq): Vanmaekelbergh, D.; Oskam, G. Debye Institute, Condensed Matter, University of Utrecht, The Netherlands, personal communication.

(19) Koval, C. A.; Howard, J.; Torres, R.; To, T. In *Proceedings of the Sixteenth DOE Solar Photochemistry Research Conference*; Division of Chemical Sciences, Office of Basic Energy Studies, U.S. Department of Energy, CONF-9205243; National Technical Information Service: Springfield, VA; 1992; p 129.

(20) Allongue, P.; Blonkowski, S. *J. Electroanal. Chem.* **1991**, *316*, 57; **1991**, *317*, 77.

(21) Howard, J. N.; Koval, C. A. *Anal. Chem.* **1991**, *63*, 2777.

(22) Kwak, J.; Bard, A. J. *Anal. Chem.* **1989**, *61*, 1221.

(23) Mirkin, M. V.; Bard, A. J. *Anal. Chem.* **1992**, *64*, 2293.

(24) Lewis, N. S. *Annu. Rev. Phys. Chem.* **1991**, *42*, 543.

(25) Gerischer, H. *Z. Phys. Chem. (Munich)* **1960**, *26*, 223.

(26) Gerischer, H. *Z. Phys. Chem. (Munich)* **1960**, *27*, 48.

(27) Marcus, R. A. *J. Chem. Phys.* **1956**, *24*, 966.

(28) Marcus, R. A. *Can. J. Chem.* **1959**, *37*, 155.

(29) Marcus, R. A. *J. Chem. Phys.* **1965**, *43*, 679.

(30) Myamlin, V. A.; Pleskov, Y. V. *Electrochemistry of Semiconductors*; Plenum: New York, 1967.

(31) Gerischer, H. *J. Phys. Chem.* **1991**, *95*, 1356.

(32) Schafer, H. *Chemical Transport Reactions*; Academic Press: New York, 1964.

(33) Wipf, D. O.; Bard, A. J. *J. Electrochem. Soc.* **1991**, *138*, 469.

(34) Zhou, F.; Unwin, P. R.; Bard, A. J. *J. Phys. Chem.* **1992**, *96*, 4917.

(35) Pierce, D. T.; Unwin, P. R.; Bard, A. J. *Anal. Chem.* **1992**, *64*, 1795.

(36) Tributsch, H. In *Structure and Bonding*; Springer-Verlag: Berlin, 1982; Vol. 49, p 127.

(37) Beal, A. R.; Liang, W. Y.; Hughes, H. P. *J. Phys. C. Solid State Phys.* **1976**, *9*, 2449.

(38) Kautek, W.; Gerischer, H. *Ber. Bunsen-Ges. Phys. Chem.* **1980**, *84*, 645.

(39) (a) Wipf, D. O.; Bard, A. J. *J. Electrochem. Soc.* **1991**, *138*, L4. (b) Bard, A. J.; Fan, F.-R. F.; Pierce, D. T.; Unwin, P. R.; Wipf, D. O.; Zhou, F. *Science* **1991**, *254*, 68.

(40) Kautek, W.; Gerischer, H.; Tributsch, H. *Ber. Bunsen-Ges. Phys. Chem.* **1979**, *83*, 1000.

(41) Canfield, D.; Furtak, T.; Parkinson, B. A. *J. Appl. Phys.* **1980**, *51*, 6018.

(42) De Angelis, L.; Scafe, E.; Galluzzi, F.; Fornarini, L.; Scrosati, B. *J. Electrochem. Soc.* **1982**, *129*, 1237.

(43) Bard, A. J.; Faulkner, L. R. *Electrochemical Methods; Fundamentals and Applications*; John Wiley & Sons: New York, 1980.

(44) McEvoy, A. J.; Etman, M.; Memming, R. *J. Electroanal. Chem.* **1985**, *190*, 225.

(45) Finklea, H. O.; Avery, S.; Lynch, M.; Furtsch, T. *Langmuir* **1987**, *3*, 409.

(46) Chazaviel, J. N. *J. Electroanal. Chem.* **1987**, *233*, 37.

(47) (a) Gronet, C. M.; Lewis, N. S.; Cogan, G. W.; Gibbons, J. F. *Proc. Natl. Acad. Sci. U.S.A.* **1983**, *80*, 1152. (b) Rosenbluth, M. L.; Lewis, N. S. *J. Am. Chem. Soc.* **1986**, *108*, 4689.

(48) Lewis, N. S. *J. Electrochem. Soc.* **1984**, *131*, 2496.

(49) Gibbons, J. F.; Cogan, G. W.; Gronet, C. M.; Lewis, N. S. *Appl. Phys. Lett.* **1984**, *45*, 1095.

(50) Mandler, D.; Bard, A. J. *Langmuir* **1990**, *6*, 1489.

(51) Fan, F.-R. F.; Bard, A. J. *J. Electrochem. Soc.* **1981**, *128*, 945.